Eur. Phys. J. B **1**, 11–17 (1998)

**THE EUROPEAN PHYSICAL JOURNAL B**



# The electronic structure of $(C_{59}N)_2$ from high energy spectroscopy

S. Haffner[1,a], T. Pichler[1], M. Knupfer[1], B. Umlauf[1], R. Friedlein[1], M.S. Golden[1], J. Fink[1], M. Keshavarz-K.[2], C. Bellavia-Lund[2], A. Sastre[2], J.C. Hummelen[2], and F. Wudl[2]

[1] Institute for Solid State and Materials Research (IFW) Dresden, 01171 Dresden, Germany
[2] Institute for Polymers and Organic Solids, Department of Chemistry and Materials, University of California, Santa Barbara, California 93106, USA

Received: 25 August 1997 / Revised: 22 September 1997 / Accepted: 16 October 1997

**Abstract.** We report the results of a detailed study of the occupied and unoccupied electronic structure of dimers of the new heterofullerene $C_{59}N$ by means of photoemission and electron energy-loss spectroscopy. A close similarity is found between the electronic structures of pristine $(C_{59}N)_2$ and $C_{60}$ with an additional broadening of the spectra in the former due to the distortion of the fullerene cage caused both by dimerization and the chemical substitution. Both the occupied and unoccupied electronic states, as well as the interband transitions between them, attest to the high degree of molecular character retained in the solid state. Comparison of the shake-up structures in the C1s and N1s X-ray photoemission spectra confirm that the highest lying occupied states in the heterofullerene have a strong degree of N character, whereas the lowest lying unoccupied states have mainly C character. We also present the optical conductivity of the heterofullerene (derived from the loss function), which shows an optical gap of 1.4 eV, some 0.4 eV smaller than that of $C_{60}$.

**PACS.** 71.20.Tx Fullerenes and related materials; intercalation compounds – 79.60.Fr Polymers; organic compounds – 78.90.+t Other topics in optical properties, condensed matter spectroscopy and other interactions of particles and radiation with condensed matter

## 1 Introduction

The discovery of metallic behaviour and superconductivity in alkali metal intercalated fullerene solids has led to great interest in the electronic structure of doped fullerene compounds, so much experimental work on exohedral, endohedral and derivatized fullerenes has been carried out including in the field of high energy spectroscopies such as photoemission spectroscopy (PES) and electron energy-loss spectroscopy (EELS) [1–3].

Another possible method of doping fullerenes is by the replacement of carbon atoms with atoms of lower, or higher, valency. This "on-ball" doping leads to so-called heterofullerenes, which are the last, as yet relatively unexplored, fullerene sub-type. Though heterofullerenes $C_{60-n}B_n$ and $C_mN_n$ had been prepared in molecular beam experiments as early as 1991 [4,5], production of a heterofullerene in macroscopic quantities was not accomplished until 1995, when $C_{59}N$ was isolated in the form of its dimer $(C_{59}N)_2$ [6] using an organic synthesis route. This development then enabled the study of heterofullerenes in the solid state. The structure of the $C_{59}N$ dimer is shown in Figure 1a. The dimer bond is a single bond between the carbon atoms labelled C′ (directly adjacent to the nitrogen atom, see Fig. 1b). Starting from as-prepared material, crystalline $(C_{59}N)_2$ can be obtained from an o-dichlorobenzene solution, from which, after drying rapidly

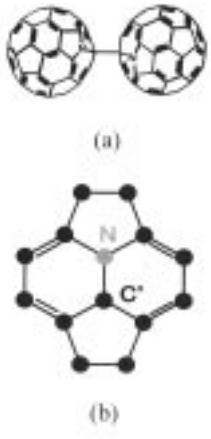


**Fig. 1.** (a) Molecular structure of the $C_{59}N$ dimer and (b) bonding configuration in the vicinity of the $C' - C'$ dimer bond (from [6]).

[a] e-mail: haffner@ifw-dresden.de

and dissolving again in $CS_2$, $(C_{59}N)_2$ can be recrystallized [7]. In an X-ray powder diffraction study [8] it was confirmed that the sublimed heterofullerene is built of $C_{59}N$ dimers, which sit on the sites of a monoclinic c-centered Bravais lattice (lattice parameters: $a = 17.25$ Å, $b = 9.96$ Å, $c = 19.45$ Å, $\beta = 124.32°$, $T = 295$ K), giving the structure a symmetry described by the space group C2/m. It is therefore isostructural to the metastable quenched dimer phase of $Rb_1C_{60}$.

In this contribution we report detailed photoemission and electron energy-loss spectroscopic studies of pristine $(C_{59}N)_2$.

## 2 Experimental

Our starting material was pristine $(C_{59}N)_2$ recrystallized by the procedure described in Section 1. $(C_{59}N)_2$ films were prepared in ultra high vacuum (UHV) by evaporation from an $Al_2O_3$ crucible. $(C_{59}N)_2$ seems to be unstable in UHV at temperatures higher than $\sim$ 200 °C. Exposure to higher temperatures for a few hours causes irreversible changes in the material which make it impossible to evaporate, even at temperatures as high as 900 °C, which is the maximum temperature we could apply. Degassing was therefore carried out at only 200 °C, but for at least 48 hours. In order to minimize the period of time at which the material was at elevated temperature, it was heated to evaporation temperature in a few minutes and evaporation was carried out in a temperature gradient as quickly as possible, regardless of the resulting film morphology. The evaporation temperature was 560 °C for the very first evaporation and increased up to 650 °C in subsequent evaporations before further evaporation became impossible. In this paper only results for material evaporated in the temperature range 560−600 °C will be shown. The pressure during evaporation never exceeded $5 \times 10^{-8}$ mbar. Characterization of films prepared under such conditions using mid-infrared and optical absorption spectroscopy showed no signs of remaining $CS_2$ solvent, $C_{60}$, or other contamination. Electron diffraction studies in the electron energy-loss spectrometer and in a transmission electron microscope showed diffraction patterns consistent with the reported monoclinic structure [8].

For EELS 1000−1500 Å thick films were prepared by sublimation onto KBr single crystals. Subsequently, the KBr substrate was dissolved in distilled water and the free-standing films were then mounted on electron microscope grids and transferred into the EELS system, which has a base pressure of $2 \times 10^{-10}$ mbar. The exposure of the sample surface to air during preparation represents no problem because of the bulk sensitivity of EELS in transmission. EELS measurements were performed in transmission using a 170 keV spectrometer described elsewhere [9]. Three different sets of energy and momentum resolutions were chosen: 340 meV and 0.12 Å$^{-1}$ for the N1s core level excitations, 160 meV and 0.1 Å$^{-1}$ for the C1s core level excitation measurements and 110 meV and 0.05 Å$^{-1}$ for the measurements of the loss function in the low energy region. The quasi-elastic line was subtracted from the measured loss functions.

$(C_{59}N)_2$ films for ultraviolet photoemission spectroscopy (UPS) or X-ray photoemission spectroscopy (XPS) were evaporated over a period of about 2 minutes onto freshly evaporated gold or copper films, respectively. A thickness of approximately 100 Å was chosen for the films for UPS in order to prevent charging effects. Evaporation of films for XPS was repeated until no substrate signal could be detected in the photoelectron spectrum. The films were then transferred under UHV conditions to the UPS and XPS spectrometers, which have a base pressure of $1.2 \times 10^{-10}$ mbar and $5 \times 10^{-11}$ mbar, respectively. UPS was carried out with He I (21.2 eV) and He II photons (40.8 eV), the latter from a microwave powered source utilizing the electron cyclotron resonance condition [10]. The photoelectrons were analyzed using a commercial 100 mm mean radius hemispherical sector analyzer giving a total energy resolution of 150 meV. Binding energies were calibrated with respect to the work function of the spectrometer, which itself was measured using the Fermi edge of a clean evaporated gold film. Weak He-satellites [11] are present in the He I radiation (He I$\beta$: 23.09 eV, He I$\gamma$: 23.743 eV), which can be satisfactory subtracted using 1.5 and 0.15% for the relative intensities of the He I$\beta$ and He I$\gamma$ satellite radiation with respect to the He I$\alpha$ main line. He II satellites (He II$\beta$: 48.372 eV, He II$\gamma$: 51.017 eV) were subtracted using 10 and 2% for the relative intensities of the satellites with respect to the main line. Because of the strength of the He II satellites, satellite subtraction is difficult and the results of the correction procedure are not as good as for the He I satellites. Prior to satellite subtraction a constant background was removed and the spectra were corrected for analyzer transmission, which was taken to be proportional to the inverse of the kinetic energy of the photoelectrons. XPS was carried out in a PHI 5600 CI spectrometer equipped with a monochromated AlK$\alpha$ source. The total energy resolution was 400 meV. A constant background has been subtracted from the spectra with no satellite subtraction being necessary because of the use of monochromated radiation. All measurements shown here were carried out at room temperature.

## 3 Results and discussion

### 3.1 Occupied electronic structure: valence band photoelectron spectra

In this section the results on the occupied electronic valence band structure of pristine $(C_{59}N)_2$ will be presented and compared to spectra of $C_{60}$. Photoemission spectroscopy gives a measure of the matrix element weighted density of occupied states (DOS) with the restriction that the spectrum is representative for the ionized final state which is not necessarily the ground state of the neutral system [12]. The photoionization cross-sections [13] for the orbitals making up the valence band (C2p, C2s, N2p, N2s) are different and photon energy dependent, so one is not necessarily measuring the total DOS, but one dominated

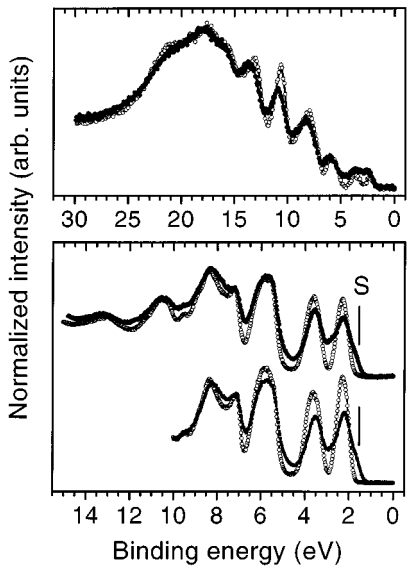


**Fig. 2.** Lower panel: He I (lower) and He II (upper) valence band UPS spectra of $(C_{59}N)_2$ (•) and $C_{60}$ (○). Upper panel: valence band XPS spectra of $(C_{59}N)_2$ (•) and $C_{60}$ (○) recorded with AlK$\alpha$ photons.

by the partial DOS of the orbitals whose cross-sections are greatest at the photon energy used. In particular, using He I ($h\nu = 21.2$ eV) radiation, the N2p and C2p-derived partial DOS are predominantly seen in the photoemission spectra, while for AlK$\alpha$ ($h\nu = 1486.6$ eV) photons the N2s and C2s-derived partial DOS dominate. For He II ($h\nu = 40.8$ eV) photons the N2p and C2p-derived partial DOS are still dominating the photoelectron spectrum but the N2s and C2s-derived partial DOS contribute significantly more than in the case of He I. The He II photoelectron spectrum represents therefore the best approximation of the total DOS of the data measured here.

In Figure 2, the He I, He II and AlK$\alpha$ photoelectron spectra of pristine $(C_{59}N)_2$ and $C_{60}$ are shown. The photoelectron spectra recorded with He resonance radiation are normalized to the peak at 7.15 eV binding energy, which belongs to mainly $\sigma$-derived molecular orbitals (MO's), whose height is proportional to the number of $\sigma$ bonds per unit cell. It is obvious from the figure that the He I and He II photoelectron spectra of $(C_{59}N)_2$ are very similar to that of $C_{60}$, showing five (He I) or seven (He II) strong, sharp features of similar shape at approximately the same binding energies. In the case of $C_{60}$, spectral weight within $\sim$ 5 eV of the highest occupied level is derived from C$-\pi$ orbitals, while those features between $\sim$ 5 eV and $\sim$ 12 eV of the highest occupied level are mainly derived from $\sigma$ hybrids [14]. The close similarity of the $(C_{59}N)_2$ and $C_{60}$ photoelectron spectra suggests that the same is true for the corresponding features in the $(C_{59}N)_2$ spectra. But there are also differences. The aforementioned strong features all show some broadening compared to $C_{60}$. This broadening originates from the distortion of the fullerene cages of the $(C_{59}N)_2$ dimers caused by the dimerization and the partial substitution of carbon atoms by nitrogen atoms. Consequently, not all carbon sites are equivalent in $(C_{59}N)_2$ molecules (see Fig. 1) in contrast to $C_{60}$ monomers ($(C_{59}N)_2$ has 30 $^{13}$C-NMR lines, space group $C_{2h}$ instead of $I_h$ for $C_{60}$ [6]), thus much of the degeneracy of the states is lifted. In addition, if the distortion of the fullerene cages due to substitution and dimerization is strong enough, it would cause a further separation of the individual MO's from each other, which, though not resolved in our experiment, is large enough to manifest itself in a broadening of the peaks.

The HOMO of $(C_{59}N)_2$ is not contained in a peak as in $C_{60}$ but in a shoulder at $\sim$ 1.5 eV binding energy (labelled S in Fig. 2) which is not present in $C_{60}$. As shown in reference [15], this shoulder is mainly derived from N$-\pi$ orbitals and the $\pi$ orbitals of the carbon atoms which establish the dimer bond. This is supported by the calculated nitrogen-derived partial DOS and the calculated spatial distribution of the HOMO-derived electron density [15]. There it was shown that the nitrogen-derived partial DOS has a peak at the energy where the shoulder is located and the spatial distribution of the HOMO-derived electron density shows a large amplitude at the nitrogen atoms as well as between the carbon atoms labelled C$'$ in Figure 1. The slight decrease of the spectral weight of feature S in the He II photoemission spectrum (compared to the He I spectrum), despite the increased N2p photoionization cross-section can be explained by the decrease of the C2p photoionization cross-section as well as the strong dependence of the relative intensities in fullerene photoelectron spectra on the photon energy caused by the molecular nature of the photoemission final state [16,17]. The top panel in Figure 2 shows AlK$\alpha$ photoelectron spectra of $(C_{59}N)_2$ and $C_{60}$. The spectra are normalized to have the same integrated intensity in the energy range shown. Again the spectra are very similar. Nine peaks derived mainly from C$-\pi$ and C$-\sigma$ orbitals can be seen at approximately the same binding energies with an additional broadening in the case of $(C_{59}N)_2$ because of the distortion of the fullerene cage (see discussion above). The peaks sit on broad $\sigma$-derived bands [18] which peak at $\sim$ 18 eV binding energy and span a total width of 27 eV.

### 3.2 Unoccupied electronic structure: EELS core level excitation spectra

We have measured the C1s and N1s core level excitation spectra of $(C_{59}N)_2$ to determine the matrix element weighted C2p and N2p-derived unoccupied partial DOS. In Figure 3 the C1s core level excitation spectra of pristine $(C_{59}N)_2$ and $C_{60}$ are presented. The spectra are normalized to the step-like edge at $\sim$ 290.5 eV excitation energy, which is due to transitions into the first antibonding $\sigma^\star$ MO. It is again clear that the $(C_{59}N)_2$ and $C_{60}$ C1s core level excitation spectra are closely related in the sense that both show similar features at roughly the same excitation energies. Thus, a common electronic origin is assumed: the first four features in the $(C_{59}N)_2$ spectrum are therefore ascribed to transitions into antibonding $\pi^\star$ MO's,

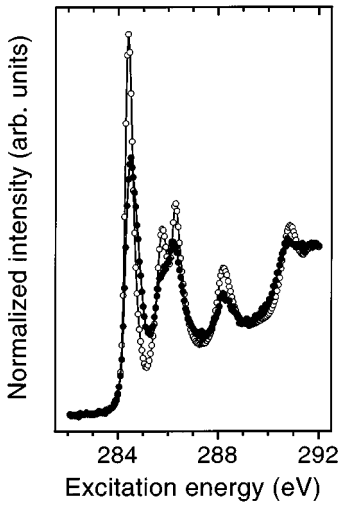


**Fig. 3.** EELS C1s core level excitation spectra of $(C_{59}N)_2$ (•) and $C_{60}$ (○).

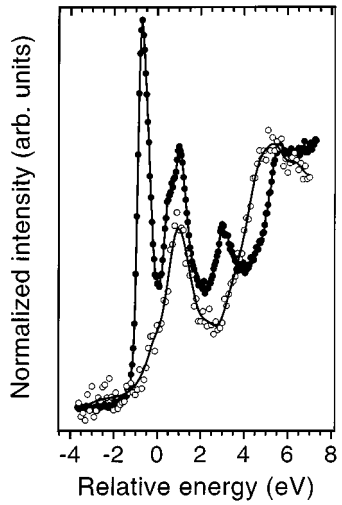


**Fig. 4.** Comparison of the EELS C1s (•) and N1s (○) core level excitation spectra of pristine $(C_{59}N)_2$. The spectra are plotted on an energy scale relative to the respective 1s core level binding energies (see text for details).

while spectral weight at and after the step-like edge at 290.5 eV excitation energy is, as mentioned above, mainly attributed to transitions into the $\sigma^\star$ MO's [3]. The only major difference between the spectra is that an additional broadening occurs for $(C_{59}N)_2$ which can again be explained by the distortion of the fullerene cage caused by the dimerization and the partial substitution of carbon atoms by nitrogen atoms, as discussed earlier. In a first approximation (neglecting excitonic effects), these core level excitation spectra give a measure of the site selected unoccupied DOS, an assessment which is supported by the excellent agreement between the C1s excitation spectrum of $(C_{59}N)_2$ and the calculated ground state electronic levels of the heterofullerene dimer presented in reference [15].

The N1s and C1s core level excitation spectra of $(C_{59}N)_2$ are shown together in Figure 4. The spectra are plotted against a relative energy scale which uses the C1s and N1s core level binding energies (C1s: 285.2 eV, N1s: 400.7 eV) as energy zero and are normalized at the $\sigma^\star$ edges at $\sim 4$ eV (N1s) and $\sim 5.4$ eV (C1s) on the relative energy scale. Qualitatively, the N1s core level excitation spectrum can be described in a similar manner as the C1s core level excitation spectrum: the edge at $\sim 4$ eV relative energy is assigned to transitions into the N2p contributions to the first $\sigma^\star$ MO, while the spectral weight between $-1$ eV and 4 eV relative energy has its origin in transitions into N2p contributions to $\pi^\star$ MO's. But one must bear in mind that in the case of the N1s core level excitation spectrum, because of the site-selectivity of this method, only unoccupied MO's which have non-negligible amplitude in the vicinity of the nitrogen sites will be probed, whereas in the C1s core level excitation spectrum such a spatial restriction hardly exists, because there are carbon atoms present practically all over the $C_{59}N$ ball. It is evident from Figure 4 that the lowest unoccupied MO's of the heterofullerene dimer are dominated by contributions from C$-\pi$ orbitals. The first significant contributions from N$-\pi$ orbitals are at $\sim 1.2$ eV relative energy. Thus upon consideration of the photoemission spectra (Fig. 2) and the core level excitation spectra (Figs. 3 and 4), and in combination with the results of calculations [15], the following picture of the low lying electronic states in $(C_{59}N)_2$ can be arrived at:

- the highest lying occupied states are energetically close to, but are shifted to lower binding energy with respect to the HOMO of pure $C_{60}$;
- the heterofullerene HOMO is spatially located mainly on the N and C′ atoms/intermolecular bond;
- the energy distribution of the lowest lying unoccupied states, however, resemble closely those of $C_{60}$ and are of almost pure C$-\pi$ character. This last point follows from the fact that the heterofullerene LUMO states have negligible weight at the N and C′ sites, and are situated mainly at the opposite end of the $C_{59}N$ molecules to the intermonomer bond.

The more mixed C$-\pi$/N$-\pi$ character of the $\pi^\star$ MO's between 0 and 4 eV relative energy seen in Figure 4 may be a signal for the sharing of (nitrogen) charge with the C′ carbon atoms which is necessary to establish the dimer bond.

### 3.3 Core level photoelectron spectra and valence band excitations

As mentioned briefly above, the final state in photoemission is not necessarily the ground state of the neutral system. This is particularly pertinent in core level photoemission upon which all outer electrons experience an effective nuclear charge increased by one in the final state. In this case, interband transitions can occur. Such transitions appear as so-called shake-up structures on the high binding energy side of the main core level line and contain valuable information about the occupied and unoccupied electronic structure near the chemical potential. In principle, the information obtained in a shake-up spectrum parallels

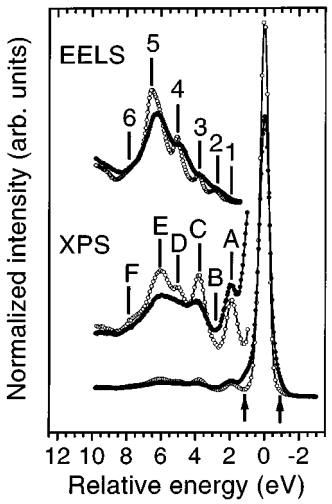


**Fig. 5.** C1s XPS spectra of $(C_{59}N)_2$ (•) and $C_{60}$ (○) recorded with AlK$\alpha$ photons. The XPS shake-up structures on the high binding energy sides of the C1s main lines of $(C_{59}N)_2$ (•) and $C_{60}$ (○) are shown on a vertically expanded scale. The energy-zero of the XPS spectra corresponds to the C1s binding energy. Uppermost: EELS loss functions of $(C_{59}N)_2$ (•) and $C_{60}$ (○). The EELS and XPS spectra are offset vertically.

that of the loss function which can be measured using EELS. For the latter, however, dipole selection rules apply at low momentum transfer and hence comparison of the shake-up spectra with the corresponding loss function can give information about the character of the interband transitions involved.

The C1s core level photoelectron spectra (XPS spectra) and loss functions of $(C_{59}N)_2$ and $C_{60}$ measured using EELS in transmission are plotted against a relative energy scale in Figure 5. The zeros of the relative energy scales of the XPS and EELS spectra are the binding energies of the C1s main line and zero energy-loss, respectively. The C1s binding energies from XPS are 285.2 eV for $(C_{59}N)_2$ and 285.0 eV for $C_{60}$. The core level spectra are normalized to have equal spectral weight (including shake-up's). The loss functions were normalized *via* a Kramers-Kronig analysis upon application of the oscillator strength sum-rule [19]. Comparison of the main lines of the $(C_{59}N)_2$ and $C_{60}$ photoelectron spectra reveals major differences. The $C_{60}$ peak is symmetric with a full width at half maximum (FWHM) of $\sim$ 0.5 eV, which arises from a combination of the spectrometer resolution (400 meV) and the lifetime of the core hole ($\sim$ 300 meV). For $(C_{59}N)_2$, the peak is broader (FWHM $\sim$ 0.7 eV) and has an asymmetric shape especially at the base of the peak where weak additional shoulders (marked by arrows in Fig. 5) are detectable. The broadening of the C1s main line of $(C_{59}N)_2$ in comparison to that of $C_{60}$ can be explained both by the distortion of the fullerene cage in the dimer (see the discussion Sect. 3.1), as well as by the presence of the electronegative N atom, which also gives rise to additional shoulders at the base of the C1s peak attributable to the carbon atoms in its immediate vicinity. Regarding the loss functions and the satellite structures on the high binding energy side of the main lines of the C1s XPS spectra, $(C_{59}N)_2$ and $C_{60}$ are very similar besides an additional broadening in the case of $(C_{59}N)_2$. The origin of the features in the $(C_{59}N)_2$ loss function and shake-up spectrum can therefore be addressed in the same way as for $C_{60}$ [3,20]. The six features recognizable in the $(C_{59}N)_2$ loss function (labelled 1 to 6) belonging to transitions between the $\pi$ and $\pi^\star$ MO manifolds and have (except for peak 2 - labelled B in the shake-up spectrum) clear corresponding counterparts in the XPS shake-up spectrum (labelled A, C, D, E and F). Apart from the relatively small weight of feature B in the shake-up spectra, the most striking difference between the loss functions and the shake-up spectra is the intensity of feature 1. The onset of the loss function has very low intensity, whereas peak A in the shake-up spectra is intense. This is a clear indication that this lowest transition has monopole character and is dipole forbidden. In $C_{60}$, the lowest transition corresponds to the dipole-forbidden "gap" transition between the $h_u$ (HOMO) to the $t_{1u}$ (LUMO) [3,20]. For $(C_{59}N)_2$, this corresponds to the lowest energy transition possible between MO's which have significant weight at the carbon sites of the heterofullerene. As discussed above, the HOMO of $(C_{59}N)_2$ lies at lower binding energy than that of $C_{60}$ and has a high degree of N character. Nevertheless, the vast majority of the low lying occupied states having C character correspond more to the HOMO of unsubstituted $C_{60}$. This is consistent with the fact that peak A occurs at the same energy in the shake-up spectra of both fullerenes. In general, the occurrence of valence band excitations with pronounced monopolar or dipolar character shows that the molecular nature is retained in the occupied and unoccupied electronic structure of pristine solid $(C_{59}N)_2$, which like pristine $C_{60}$ must be regarded as a molecular solid with only weak interaction between the dimers.

The substitution of the N into the heterofullerene now gives us the possibility of measuring the excitations of the system in a site specific manner. By measuring the shake-up satellites of the N1s core level, we can selectively study the transitions between MO's with significant weight at the N site. Figure 6 shows a comparison of the shake-up regions of the C1s and N1s XPS spectra of $(C_{59}N)_2$. In both cases, the solid line is intended as a guide to the eye. In each case, the energy zero corresponds to the binding energy of the XPS main line (N1s: 400.7 eV, C1s: 285.2 eV) and the spectra are normalized to have the same total area. Comparison of the C1s and N1s shake-up spectra reveals a marked difference. In contrast to the C1s shake-up spectrum, the N1s shake-up spectrum has no peak at $\sim$ 1.8 eV relative energy (peak A in Fig. 5). This is once more clear evidence in support of the calculated spatial distributions of the electronic states on either side of the chemical potential [15]. Thus, as the LUMO states of the heterofullerene have practically zero weight at the N site, the sudden injection of a core hole at this site cannot be screened by a transition between the high lying occupied states and the lowest unoccupied molecular orbitals of the heterofullerene. Above $\sim$ 3 eV relative energy, the C1s and N1s shake-up spectra look similar with peaks

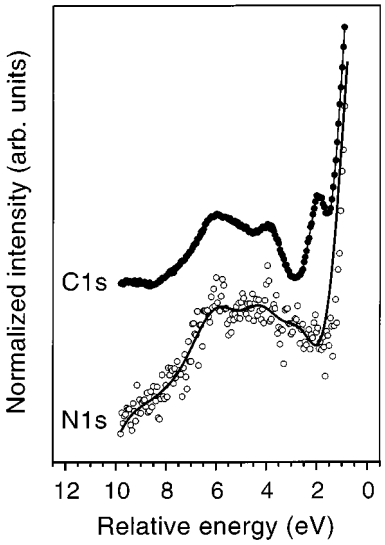


**Fig. 6.** C1s (•) and N1s (○) XPS shake-up spectra of pristine $(C_{59}N)_2$ recorded with AlK$\alpha$ photons. The shake-up spectra are offset vertically and are plotted on an energy scale relative to the respective 1s core level binding energies (see text for details).

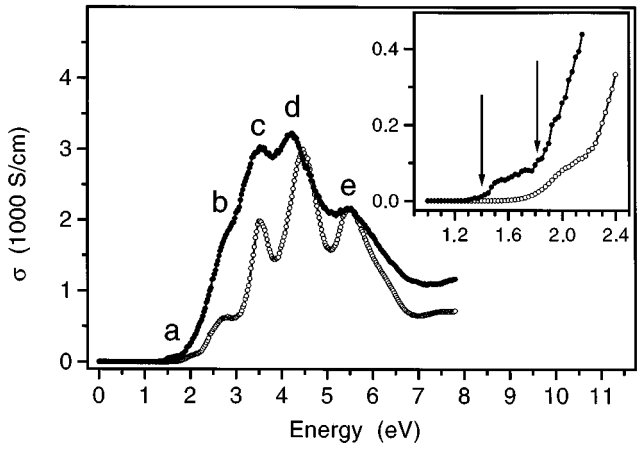


**Fig. 7.** Optical conductivities of pristine $(C_{59}N)_2$ (•) and $C_{60}$ (○) derived from a Kramers-Kronig analysis of the measured loss functions. The inset shows the onset region in more detail.

at $\sim 4$ eV and $\sim 6$ eV. These features involve transitions into $\pi^\star$ levels of higher energy than the LUMO, or represent excitation of the so-called $\pi$-plasmon, showing that the MO's involved have significant weight at the nitrogen site.

The loss function from EELS (as shown in Fig. 5) is also the basis for the determination of the dielectric function *via* a Kramers-Kronig analysis [19], from which the optical conductivity can be derived. This quantity is directly proportional to the matrix-element-weighted joint density of states. Figure 7 shows the optical conductivity of $(C_{59}N)_2$ and $C_{60}$ derived as described above. The corresponding loss functions are normalized according to the oscillator strength sum-rule [19]. Both curves are similar in overall shape, showing five features (labelled a to e) belonging to dipolar transitions between the $\pi$ and $\pi^\star$ MO manifolds. The features of the $(C_{59}N)_2$ spectrum are again broadened compared to $C_{60}$ and peak d is shifted to lower energy. Of particular interest is the difference between the onsets of the spectra (feature a): 1.8 eV for $C_{60}$ compared to 1.4 eV for $(C_{59}N)_2$. Calculations of Kohn-Sham energy levels [21] predict a decrease of the magnitude of the gap of $C_{60}$ to $(C_{59}N)_2$ by 0.4 eV, which nicely matches our experimental result for the optical gap and the existence of a shoulder at lower binding energies in the photoemission experiments.

## 4 Conclusions

In this paper we have discussed detailed measurements of the electronic structure of dimers of the heterofullerene $C_{59}N$ in the solid state using high energy spectroscopy. An electronic structure generally similar to that of monomer $C_{60}$ is found, with an additional broadening caused both by the dimerization and the partial substitution of carbon atoms by the nitrogen atoms. However, the valence band photoemission and EELS core level excitation spectra presented here show that in $(C_{59}N)_2$, the lowest lying bonding $\pi$ MO's ($\sim 1.5$ eV binding energy) are mainly derived from N$-\pi$ and C$'-\pi$ orbitals (C$'$ being the carbon atoms between which the dimer bond is found). In contrast, the lowest lying unoccupied MO's in the heterofullerene are dominated by $\pi$ contributions from carbon atoms located well away from the dimer bond, and are therefore much more similar to the LUMO states of $C_{60}$. This result is confirmed by calculations [15], as well as by the remarkable absence of valence band excitations related to HOMO-LUMO transitions in the N1s shake-up spectrum.

Comparison of the $(C_{59}N)_2$ C1s shake-up spectrum with the EELS loss function shows that the transitions involved in valence band excitations of $(C_{59}N)_2$ have pronounced monopolar or dipolar character. Thus pristine $(C_{59}N)_2$ should be regarded as a molecular solid with only weak interactions between the dimers. In addition, the optical conductivity of $(C_{59}N)_2$ is derived from the measured EELS loss function and an optical gap of 1.4 eV, some 0.4 eV smaller than that of $C_{60}$, is found.

We acknowledge the Bundesministerium für Bildung, Wissenschaft, Forschung und Technologie (BMBF) for financial support under contract number 13N6676/7. S.H. acknowledges the support of the DFG (Graduiertenkolleg "Struktur- und Korrelationseffekte in Festkörpern" TU-Dresden). T.P. and M.S.G. thank the European Union for funding under the 'Training and Mobility of Researchers' and 'Human Capital and Mobility' programs.

## References

1. J.H. Weaver, J. Phys. Chem. Solids **53**, 1433 (1992).
2. J.H. Weaver, D.M. Poirier, *Solid State Physics*, edited by H. Ehrenreich and F. Saepen (New York: Academic, 1994), vol. 48.

3. M.S. Golden, M. Knupfer, J. Fink, J.F. Armbruster, T.R. Cummins, H.A. Romberg, M. Roth, M. Sing, M. Schmidt, E. Sohmen, J. Phys.: Condens. Matter **7**, 8219 (1995).
4. T. Guo, C. Jin, R.E. Smalley, J. Phys. Chem. **95**, 4948 (1991).
5. T. Pradeep, V. Vijayakrisnan, A.K. Santra, C.N.R. Rao, J. Phys. Chem. **95**, 10564 (1991).
6. J.C. Hummelen, B. Knight, J. Pavlovich, R. Gonzalez, F. Wudl, Science **269**, 1554 (1995).
7. C.M. Brown, E. Beer, C. Bellavia-Lund, A.K. Cheetham, L. Christofolini, R. Gonzalez, M. Hanfland, D. Häusermann, M. Keshavarz-K., K. Kordatos, K. Prassides, F. Wudl, J. Am. Chem. Soc. **118**, 8716 (1996).
8. C.M. Brown, L. Cristofolini, K. Kordatos, K. Prassides, C. Bellavia-Lund, R. Gonzalez, M. Keshavarz-K., F. Wudl, A.K. Cheetham, J.P. Zhang, W. Andreoni, A. Curioni, A.N. Fitch, P. Pattison, Chem. Mater. **8**, 2548 (1996).
9. J. Fink, Adv. Electron. Electron Phys. **75**, 121 (1989).
10. Gammadata VUV 5010, Gammadata Maetteknik AB, Uppsala, Sweden.
11. J.A.R. Samson, *Techniques of vacuum ultraviolet spectroscopy* (New York: John Wiley & sons, 1967).
12. S. Hüfner, *Photoelectron Spectroscopy* (Berlin, Heidelberg, New York: Springer Verlag, Berlin, 1995).
13. J.J. Yeh, I. Lindau, At. Data Nucl. Data Tab. **32**, 1 (1985).
14. J.H. Weaver, J.L. Martins, T. Komeda, Y. Chen, T.R. Ohno, G.H. Kroll, R.E. Haufler, R.E. Smalley, Phys. Rev. Lett. **66**, 1741 (1991).
15. T. Pichler, M. Knupfer, M.S. Golden, S. Haffner, R. Friedlein, J. Fink, W. Andreoni, A. Curioni, M. Keshavarz-K., C. Bellavia-Lund, A. Sastre, J.C. Hummelen, F. Wudl, Phys. Rev. Lett. **78**, 4249 (1997).
16. P.J. Benning, D.M. Poirier, N. Trouillier, J.L. Martins, J.H. Weaver, R.E. Haufler, L.P.F. Chibante, R.E Smalley, Phys. Rev. B **44**, 1962 (1991).
17. J. Wu, Z.-X. Shen, D.S. Dessau, R. Cao, D.S. Marshall, P. Pianetta, I. Lindau, X. Yang, J. Terry, D.M. King, B.O. Wells, D. Elloway, H.R. Wendt, C.A. Brown, H. Hunziker, M.S. de Vries, Physica C **197**, 251 (1992).
18. D.M. Poirier, J.H. Weaver, K. Kikuchi, Y. Achiba, Z. Phys. D **26**, 87 (1992).
19. T. Pichler, M. Knupfer, M.S. Golden, R. Friedlein, S. Haffner, B. Umlauf, O. Knauff, H.-D. Bauer, J. Fink, M. Keshavarz-K., C. Bellavia-Lund, A. Sastre, J.C. Hummelen, F. Wudl, Synth. Met. **86**, 2313 (1997).
20. P.J. Benning, D.M. Poirier, T.R. Ohno, Y. Chen, M.B. Jost, F. Stepniak, G.H. Kroll, J.H. Weaver, J. Fure, R.E. Smalley, Phys. Rev. B **45**, 6899 (1992).
21. W. Andreoni, A. Curioni, K. Holczer, K. Prassides, M. Keshavarz-K., J.C. Hummelen, F. Wudl, J. Am. Chem. Soc. **118**, 11335 (1996).